

Polarization Multiplexing Dammann Grating Based on All-Dielectric Metasurface

Chenyang Wu , Xuanlun Huang , Yipeng Ji , Jiaxing Wang , and Connie J. Chang-Hasnain , *Fellow, IEEE*

Abstract—Dammann gratings (DG) have become a powerful tool for generating multi-level spectral points in speckle arrays through binary phase variation. Conventional DGs are limited to regular dot arrays, such as squares and circular rings. Emergence of metasurface-based coding technology opens new ways for ultra-thin, compact and miniaturized DGs. In this study, we present a novel polarization multiplexing DGs employing an all-dielectric metasurface. Our work introduces a DG optimization algorithm tailored for specific desired array patterns, including non-centrally symmetric arrays and arrays maximizing specific desired orders. This innovation broadens the applications of DGs in irregular arrays. Additionally, in contrast to numerous dimension sizes generated by conventional Gerchberg-Saxton (GS) algorithms, the proposed method employs silicon nanorod array with only three distinct sizes. This streamlined approach greatly enhances precision control in nanofabrication and facilitates large-scale industrial replication. Furthermore, incorporation of polarization multiplexing in DGs enhances their versatility, amplifying channel capacity and spectrum utilization, and allowing for secure encoding of private information through polarization states. The utilization of orthogonal polarization states becomes crucial for information reuse and hiding, where independent coding information is applied to orthogonally polarized light, enabling applications such as secure information reuse and hiding. Simultaneously, the method maintains exemplary performance metrics, with efficiencies and uniformities of 75% and 77%, respectively. Notably, our approach achieves effective suppression of the 0th diffraction order intensity, a crucial advancement with substantial implications for practical metasurface optics applications. The proposed method holds great promise across diverse applications, including structured light projection, optical communication and 3D imaging.

Index Terms—Dammann grating, metasurface, polarization multiplexing, structured light.

Manuscript received 23 January 2024; revised 12 February 2024; accepted 14 February 2024. Date of publication 20 February 2024; date of current version 1 March 2024. This work was supported in part by the Shenzhen Science and Technology Program under Grant KQTD20200820113053102, Grant ZDSYS20220325163600001, and Grant JSGG20220831110404008, in part by Hetao Shenzhen-Hong Kong Science and Technology Innovation Cooperation Zone Program under Grant HZQSWS-KCCYB-202203, and in part by Guangdong Major Talent Introduction Project under Grant 2021ZT09X328. (*Corresponding author: Connie J. Chang-Hasnain*)

Chenyang Wu and Xuanlun Huang are with the School of Information Science and Technology, Fudan University, Shanghai 200433, China, and also with Berxel Photonics Company Ltd., Shenzhen 518071, China (e-mail: cywu20@fudan.edu.cn; xuanlunhuang20@fudan.edu.cn).

Connie J. Chang-Hasnain is with the School of Information Science and Technology, Fudan University, Shanghai 200433, China, also with Berxel Photonics Company Ltd., Shenzhen 518071, China, also with Chinese University of Hong Kong, Shenzhen 518172, China, and also with Peng Cheng Laboratory, Shenzhen 518055, China (e-mail: connie.chang@berxel.com).

Yipeng Ji and Jiaxing Wang are with Berxel Photonics Company Ltd., Shenzhen 518071, China (e-mail: yipeng.ji@berxel.com; jiaxing.wang@berxel.com).

Digital Object Identifier 10.1109/JPHOT.2024.3367298

I. INTRODUCTION

DAMMANN grating (DG) is a kind of diffraction optical element (DOE) with spatial coordinate modulation of binary phase [1]. It enables efficient conversion of monochromatic incident light into a precisely arranged regular dot matrix with uniform intensity distribution in the far field. Originating from Dammann et al.’s pioneering work in the 1970s, DGs emerged during the exploration of multiple image reproductions, marking the initial integration of large-scale integrated circuit fabrication into optics. Subsequent developments in the 1990s introduced novel structures such as even dot matrix DGs and non-orthogonal DGs [2], [3]. Zhou et al. notably applied optimization algorithms to compute numerical solutions for Dammann gratings, spanning from 2×2 to 64×64 splitting ratios [4]. This significantly augmented the theoretical foundation and expanded the application domain of Dammann gratings. Presently, DGs find ubiquitous utility in diverse fields such as optical communication [5], [6], monocular/stereo vision 3D measurement [7], [8], and structured light projection [9], [10].

Metasurfaces, exemplifying artificial planar structural materials with sub-wavelength characteristics, exhibit the remarkable capability to precisely regulate the amplitude, phase, polarization, and spectrum of electromagnetic waves on a sub-wavelength scale [11], [12], [13]. It is widely used in metalenses [14], meta-hologram [15], high-resolution image display [16], vortex beam generator [17], information encryption/concealing [18], etc. Recently, nanograting coding technology based on metasurface provides new design path for ultra-thin, compact and miniaturized DGs [19], [20], [21], [22], [23]. Li et al. integrated the principles of geometric phase and depth phase modulation, proposing a DG based on all-silicon nanorods capable of achieving a 4×4 spot array in the far field using 32 phase levels [19]. Extending this paradigm, Yang et al. employed a silicon nanorod array to realize polarization-insensitive DGs featuring a 5×5 regular diffraction array [20]. Ni et al. designed a structured light DOE with field of view (FOV) of 120° by optimizing the size parameters of 6×6 cylindroid cells [21]. Zheng et al. utilized TiO₂ cylindrical dielectric antenna to produce a 5×5 regular diffraction array with FOV of $20^\circ \times 20^\circ$ [22]. Wu et al. used straight and helical nanorods to generate a 5×5 diffraction array in multi-wavelength [23]. Li et al. introduced a novel Hermitian-conjugate metasurface capable of scattering incident light into a cloud of random points across full 4π spherical space with compressed information density. This metasurface exhibits exceptional functionality in both transmission and reflection spaces, achieving over 4044 random

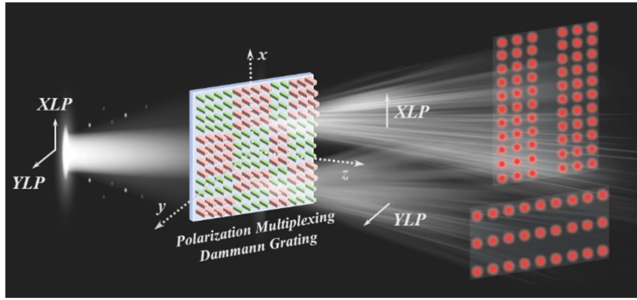


Fig. 1. Illustration of the proposed polarization multiplexing Dammann grating based on all-dielectric metasurface.

spots distributed at angles nearing 90° [24]. Despite these strides, extant research predominantly focuses on generating regular square array patterns (e.g., 4×4 , 5×5) with uniform length and width of central symmetry, neglecting specific irregular patterns such as non-uniform and non-centrally symmetric arrays, as well as arrays with maximized specific desired orders. Furthermore, prevalent studies rely extensively on computer iterative algorithms (e.g., GS algorithm, gradient descent algorithm) for phase generation, leading to numerous size parameters of the unit cell and a broad range of dimensions. This not only exacerbates challenges in precision control during nanofabrication but also poses hindrances to large-scale industrial replication.

In this study, we present the polarization multiplexing DGs utilizing an all-dielectric metasurface. Our research introduces 2D DG optimization algorithm meticulously crafted for specific array patterns, encompassing non-centrally symmetric arrays and arrays tailored to maximize specific desired orders. This methodology significantly expands the potential applications of DGs within irregular arrays. In contrast to the myriad dimension sizes generated by conventional GS algorithms, our proposed approach adopts a silicon nanorod array characterized by a mere three distinct sizes. This refined strategy not only sharpens precision control in nanofabrication but also streamlines large-scale industrial replication processes. Moreover, the integration of polarization multiplexing in DGs goes beyond mere versatility, serving to magnify both channel capacity and spectrum utilization. This capability concurrently facilitates the secure encoding of private information through polarization states. The pivotal role of orthogonal polarization states becomes apparent in scenarios of information reuse and concealment, where independent coding information is meticulously applied to orthogonally polarized light. This opens avenues for secure information reuse and discreet data transmission. Fig. 1 illustrates the proposed polarization multiplexing Dammann grating based on an all-dielectric metasurface, where XLP and YLP denote x-linear polarization and y-linear polarization incident light, respectively. Besides, the proposed method upholds exemplary performance metrics, showcasing efficiencies and uniformities of 75% and 77%, respectively. It is noteworthy that our approach achieves the effective suppression of the 0th diffraction order intensity, marking a advancement with profound implications for the practical applications of metasurface optics. We envision that our method holds promise for a diverse range of practical

applications, encompassing 3D imaging, structured light projection, optical communication and computing.

II. DESIGN AND SIMULATION

A. Structure Design and Optimization of DGs

DGs represent typical $(0, \pi)$ binary DOEs producing uniform distribution of dot array with simple structure. The optimization of DG parameters is essentially to calculate a set of coordinates of phase transition points. According to the Fourier optics theory, the light intensity distribution of each diffraction order can be calculated by Fourier transform of the transfer function $T(x)$, which can be described as Fourier series expansion. Therefore, the light field distribution I_n of the n^{th} diffraction order ($n \neq 0$) is denoted as:

$$I_n = \frac{\sin(\Delta\theta/2)}{\pi n} \sum_{k=1}^N (-1)^k \exp(-2\pi i n x_k) \quad (1)$$

and the 0th diffraction order amplitude is expressed as:

$$I_0 = 2 \sin\left(\frac{\Delta\theta}{2}\right) \sum_{k=1}^N (-1)^k x_k \quad (2)$$

wherein x_i and N are modulation coordinate and total number of normalized phase transition point, respectively; $\Delta\theta$ is the binary phase difference, i.e., π .

The 2D DG structure is obtained by multiplying and expanding the 1D DG parameters in orthogonal direction. Conventional DGs can only generate regular square array with uniform length and width of central symmetry in the far field (such as 4×4 , 5×5 , etc.), without other specific forms of irregular patterns, such as non-uniform and non-axisymmetric, or specific desired order maximized arrays, etc. Next, we propose 2D DG optimization algorithm for specific desired target array to expand the application of DGs.

Firstly, we construct two cost function $cost_x$ and $cost_y$ according to the desired target diffraction order in x and y directions, integrating diffraction efficiency with uniformity. Specifically, taking the minimization of $\pm p$ and $\pm q$ desired diffraction orders as an example, the cost function is expressed as:

$$\begin{aligned} Cost &= W [\max(I_k) - \min(I_k)]^2 + \\ &(1-W) \left\{ \sum_{k=-n}^n \left(\frac{\eta}{N} - I_k \right)^2 + \sum_{k'=\pm p, \pm q} |I_{k'}|^2 \right\} \end{aligned} \quad (3)$$

where $I_{k'}$ is the far-field light intensity distribution of $\pm p$ and $\pm q$ diffraction orders; I_k is the intensity distribution of the k^{th} diffraction order ranging from $-n$ to n , excluding $\pm p$ and $\pm q$ diffraction orders; N is the sum of the diffraction orders excluding the desired minimized diffraction orders; η is the total target diffraction efficiency; W is the weight factor ($0 \sim 1$), which is used to balance the uniformity of the diffraction array and total diffraction efficiency. By minimizing the cost function, spatial modulation coordinates of the phase transition point in x and y direction can be obtained with high diffraction efficiency

TABLE I
COORDINATES OF NORMALIZED TRANSITION POINTS IN EXAMPLE 1
AND EXAMPLE 2

<i>Example 1</i>	
x direction	0.1824, 0.2742, 0.5858, 0.6797, 0.7191, 0.8222, 0.9064
y direction	0.2075, 0.6448, 0.6674, 0.7080, 0.7480, 0.7704
<i>Example 2</i>	
x direction	0.1824, 0.2742, 0.5858, 0.6797, 0.7191, 0.8222, 0.9064
y direction	0.2075, 0.6448, 0.6674, 0.7080, 0.7480, 0.7704

and low non-uniformity. Specifically, the iterative optimization algorithm can be used to minimize the cost function, including simulated annealing (SA) and gradient descent algorithm. Take the SA algorithm as an example, the minimization optimization process of $cost_x$ is as follows:

- Step 1: Set the initial temperature $T = T_0$, and randomly generate initial solution of normalized transition point modulation coordinate x ($0 < x < 1$), and calculate $cost_x(x)$;
- Step 2: Set iterations L of each temperature T , and $T = kT$, where k indicates the rate of temperature decline ($0 < k < 1$);
- Step 3: Apply random perturbation Δx to the current solution so that a new solution is generated in its neighborhood as: $x_{new} = x + \Delta x$;
- Step 4: Determine the cost function of the new solution $cost_x(x_{new})$ and increment of the cost function: $\Delta cost_x = cost_x(x_{new}) - cost_x(x)$;
- Step 5: If $\Delta cost_x < 0$, then accept x_{new} as the new current solution. Otherwise, the probability $\exp(-\Delta cost_x/kT)$ is used to determine whether to accept x_{new} as the new current solution;
- Step 6: At temperature T , repeat L times of disturbance and acceptance process of Step 3 to Step 5;
- Step 7: Determine whether the temperature T has reached the threshold of the termination temperature; if so, terminate the algorithm to obtain the optimized modulation coordinates of the transition points; Otherwise, return to Step 3 and repeat the iterative process.

The optimization process for $cost_y$ is consistent with $cost_x$. Ultimately, the coordinates of transition points in both x and y direction are derived, and a 2D DG structure is formed by multiplying and expanding the above 1D DG parameters in orthogonal direction. To verify the feasibility of the proposed algorithm, we define two illustrative examples: *Example 1* involves the maximization of 0th to ± 7 th diffraction orders in the x direction and the maximization of ± 1 st diffraction orders (while minimizing the 0th order) in the y direction. In *Example 2*, we set out to maximize 0th to ± 15 th diffraction orders in the x direction, concurrently maximizing ± 1 st/ ± 2 th/ ± 4 th/ ± 5 th diffraction orders (while minimizing the 0th order and ± 3 rd orders) in the y direction. The proposed algorithm is then employed to compute the coordinates of phase transition points in both x and y directions, as presented in Table I.

According to the optimized coordinates from Tables I and II, the 2D DG structure for *Example 1* and *Example 2* are depicted in Fig. 2(a) and (b), respectively, where black

TABLE II
SELECTED L AND W DIMENSIONS OF THE UNIT CELL FOR POLARIZATION MULTIPLEXING DG METASURFACE

L (nm)	W (nm)	φ_x	φ_y	T_x	T_y
170	170	π	π	0.95	0.95
210	210	2π	2π	0.99	0.99
235	155	2π	0.99π	0.99	0.94
155	235	0.99π	2π	0.94	0.99

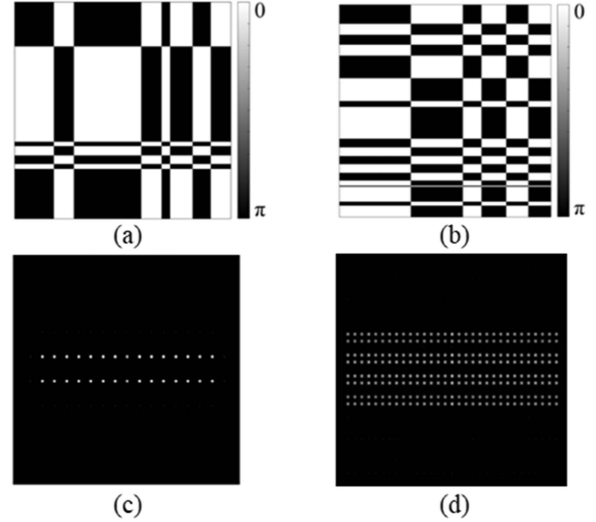


Fig. 2. 2D DG of *Example 1* (a) and *Example 2* (b) and corresponding Fourier far-field distribution of *Example 1* (c) and *Example 2* (d).

and white region denote phase values of π and 0, respectively. The far-field distribution for two examples are subsequently calculated through Fourier transform, resulting in Fig. 2(c) and (d), respectively. In Fig. 2(c), the x direction exhibits 15 dots spanning 0th to ± 7 th orders, while the y direction showcases a minimized 0th order and maximized ± 1 st orders, creating a suppression-induced vacancy at the position of the 0th order; In Fig. 2(d), the x direction exhibits 31 dots spanning 0th to ± 15 th orders, while the y direction demonstrates a vacancy at the positions of the 0th and ± 3 rd orders due to their minimization, coupled with the maximization of ± 1 st/ ± 2 th/ ± 4 th/ ± 5 th orders, resulting in a vacancy at the position of the 0th and ± 3 rd order.

Moreover, the computed DG structure can be processed by various graphic transformation methods, including but not limited to tangent transformation, rotation transformation, pattern stitching, etc. As an illustrative example, we apply tangent transformation, specifically with a 30° rotation in the horizontal direction, resulting in the new grating structures displayed in Fig. 3(a) and (b) for *Example 1* and *Example 2*, respectively. The corresponding Fourier far-field distributions are depicted in Fig. 3(c) and (d), respectively.

B. Design of Polarization Multiplexing Dammann Grating Based on Metasurface

Based on principles in the preceding section, we can obtain the desired far-field dot array distribution through elaborated

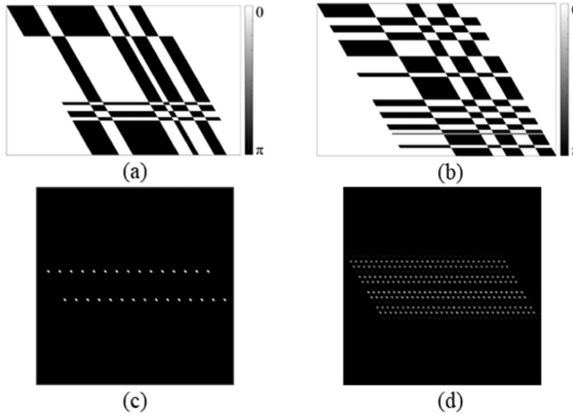


Fig. 3. 2D DG with 30° horizontal tangent transformation of *Example 1* (a) and *Example 2* (b) and corresponding Fourier far-field distribution (c) and (d).

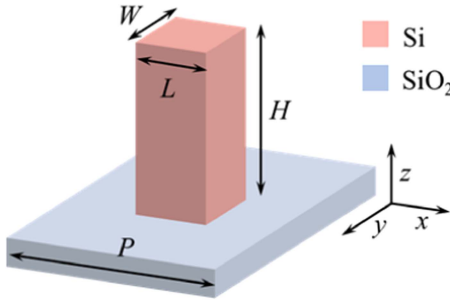


Fig. 4. Unit-cell of the proposed metasurface.

designed and optimized 2D DGs based on metasurface. Fig. 4 illustrates the unit-cell of the proposed metasurface, comprising a monolayer of amorphous silicon nanorods situated on a fused silica substrate. W , L and H denote width, length and height of the unit cell, and P is the lattice constant. Due to the strong coupling effect of amorphous silicon nanorods with incident light, each nanorod can be considered as a waveguide with both sides truncated, and the incident light scattered by each nanorod is mainly affected by the geometric parameters of the nanorod [25], [26]. In light of this, each unit cell within the lattice functions as an independent pixel for separate design considerations for simplicity. The rectangular section of the unit cell results in varying refractive indices along the length and width of the nanorod when subjected to *XLP* and *YLP* incident light. Consequently, each nanorod introduces a polarization-dependent phase shift on the incident light. Through the elaborately design of nanorod parameters and the manipulation of the phase distribution of the incident light wavefront, we can realize a phase coverage of 0 to 2π for both *XLP* and *YLP* incident light. This serves the function of polarization multiplexing, enabling the generation of diverse dot array patterns in the far field through the metasurface.

The unit cell is scanned using finite difference time domain (FDTD) simulation software (Lumerical Inc.). With the incident wavelength fixed at 940 nm, H and P are set to 750 nm and 500 nm, respectively. The background refractive index of the environment is set to 1, and the refractive index of silicon and silicon dioxide are obtained from the “Palik Optics”. The

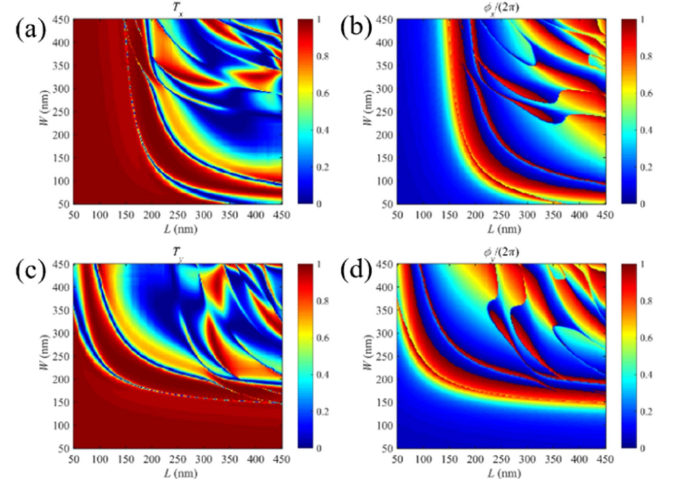


Fig. 5. Transmission and phase distribution with *XLP* incident light (a)/(b) and *YLP* incident light (c)/(d).

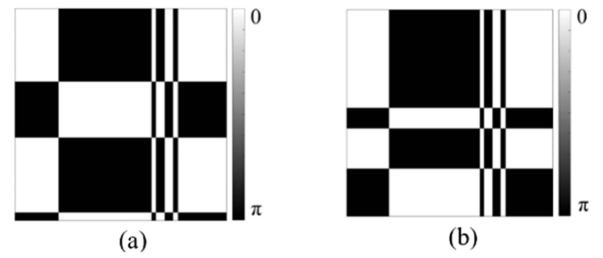


Fig. 6. 2D DG for *XLP* (a) and *YLP* (b) incident light.

scanning range of L and W spans from 50 nm to 450 nm. The transmission and phase distribution of the unit cell under *XLP* and *YLP* incident light are shown in Fig. 5, and the phase distribution has been normalized by 2π . By systematically adjusting the parameters L and W of the unit cell, a diverse array of phase coverage combinations ranging from 0 to 2π , all while maintaining high transmission, can be achieved. This allows for the generation of various desired phase distributions and far-field dot arrays under both *XLP* and *YLP* incident light.

Continuing with the analysis, we proceed to calculate the parameters of DGs based on metasurface for polarization multiplexing. Under *XLP* incident light, we set the optimization criteria as the maximization of 0th $\sim \pm 2$ nd diffraction orders in the x direction and maximization of ± 1 st diffraction orders (minimizing 0th order) in the y direction, resulting in a 5×2 dot array distribution; Similarly, under *YLP* incident light, the optimization criteria involve the maximization of ± 1 st diffraction orders (minimizing 0th order) in the x direction and maximization of 0th to ± 3 rd diffraction orders in the y direction, resulting in a 2×7 dot array distribution. The proposed 2D DG optimization algorithm is then applied to optimize the coordinates of phase transition points. The resulting calculated grating structure for *XLP* and *YLP* incident light is presented in Fig. 6(a) and (b), respectively.

To achieve the desired phase distributions under both *XLP* and *YLP* incident light, we leverage the transmission and phase distribution information presented in Fig. 5. Specifically, we

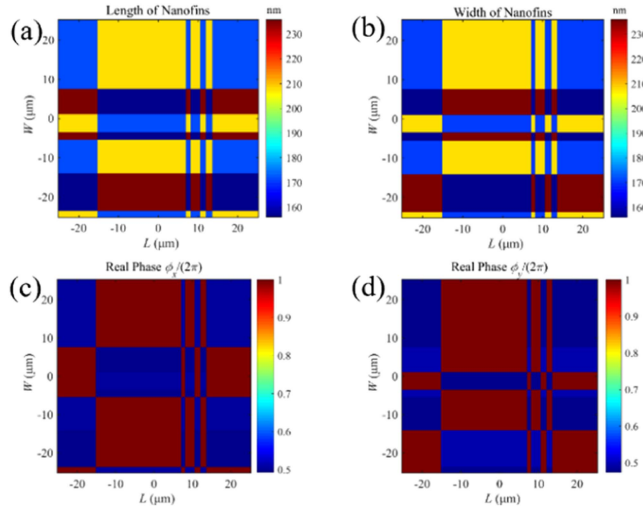


Fig. 7. Dimension distributions of L (a) and W (b) and phase distribution for XLP (c) and YLP (d) incident light.

select different parameters for L and W of the unit cells to ensure compatibility with the two types of phase distributions within a single metasurface structure. Considering phase differences of 0 and π , the permutations for a single nanorod include $\varphi_x = \pi$, $\varphi_y = \pi$; $\varphi_x = 2\pi$, $\varphi_y = 2\pi$; $\varphi_x = 2\pi$, $\varphi_y = \pi$; $\varphi_x = \pi$, $\varphi_y = 2\pi$, where φ_x and φ_y are phase values under XLP and YLP incident light, respectively. Through delicate design, we select four sets of optimized dimensions for L and W , capable of realizing the desired phase distributions for polarization multiplexing DGs with relatively high transmission. The selected dimensions are presented in Table II, where two types of dimensions are equal, and the other two types of dimensions share the same L and W . This configuration facilitates precision control during fabrication. Each period of the metasurface is comprised of 200×200 nano-bricks. Periodic boundary conditions are applied in the x and y directions. The complete dimension distributions of L and W for the metasurface corresponding to Fig. 6 are depicted in Fig. 7(a) and (b), respectively. Fig. 7(c) and (d) showcase the practical phase distribution of the metasurface for XLP and YLP incident light, respectively, demonstrating a close alignment with the designed grating structure in Fig. 6. Using a similar design methodology, we extend our calculations to polarization multiplexing DG metasurfaces generating 5×5 and 7×7 uniform dot array distributions for XLP and YLP incident light, respectively.

III. RESULTS AND DISCUSSION

Applying the proposed design approach, we utilize FDTD simulations to numerically assess the far-field diffraction distribution under XLP and YLP incident light. For the first type of polarization multiplexing DG metasurface, the normalized intensity distributions under XLP and YLP incident light are depicted in Fig. 8(a) and (c), respectively. The corresponding 3D intensity distributions are presented in Fig. 8(b) and (d), respectively. Under XLP incident light, a 5×2 dot array distribution is achieved, where 0th to ± 2 nd and ± 1 st diffraction orders

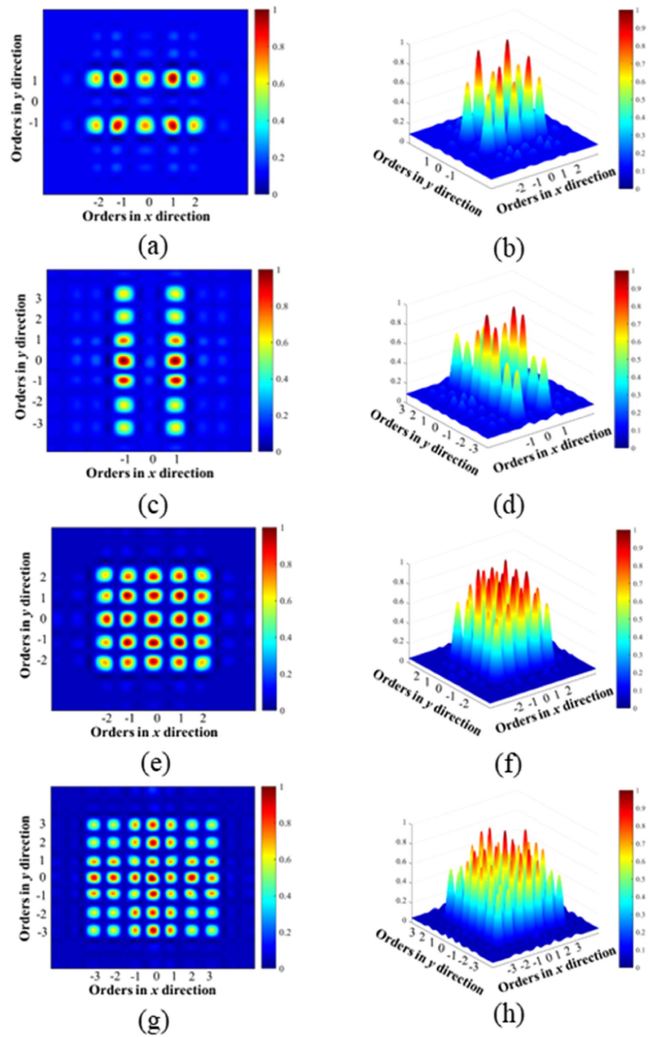


Fig. 8. Normalized intensity and 3D intensity distribution of the designed polarization multiplexing DG metasurface. Design 1 for XLP (a)/(b) and YLP (c)/(d) incident light; Design 2 for XLP (e)/(f) and YLP (g)/(h) incident light.

are generated in the x and y directions, respectively. Notably, the 0th order intensity is minimized in the y direction. Under YLP incident light, a 2×7 dot array distribution is realized, featuring ± 1 st and 0th to ± 3 rd diffraction orders in the x and y directions, respectively, with the 0th order intensity minimized in the x direction.

Similarly, for the second type of polarization multiplexing DG metasurface, uniform 5×5 and 7×7 dot array distributions are obtained under XLP and YLP incident light, as demonstrated in Fig. 8(e) and (g), respectively. The corresponding 3D intensity distributions are displayed in Fig. 8(f) and (h), respectively. These simulations affirm the effectiveness of the proposed design methodology in achieving diverse and tailored dot array distributions based on the polarization state of the incident light.

The uniformity of the dot array is quantified by the formula $1 - [\max(I_n) - \min(I_n)]/[\max(I_n) + \min(I_n)]$, where I_n represents the intensity of the n th diffraction order, and $\max(I_n)$ and $\min(I_n)$ denote the maximum and minimum intensity across all diffraction orders, respectively. The uniformity

TABLE III
UNIFORMITY OF TWO DESIGNS FOR *XLP* AND *YLP* INCIDENT LIGHT

Polarization	Design 1	Design 2
XLP	79.66%	78.82%
YLP	75.07%	74.61%

TABLE IV
COMPARISON BETWEEN RELATED WORK ON 2D DIFFRACTION DOT ARRAY GENERATION BASED ON METASURFACE

Ref.	Nanorods parameters		Conversion efficiency	Uniformity	Far field dot array pattern
	Height (nm)	Types			
19	920	1	50%	95%	4x4
20	1000	2	41%	50%	5x5
21	850	36	59%	75%	9x9
22	1300	2	60%	67%	5x5
23	1000	2	50%	60%	5x5
Our work	750	3	75%	73%	5x5/7x7; 2x7/5x2 (Suppression of 0 th order); Maximization of specific orders

for the two designs under *XLP* and *YLP* incident light are calculated and presented in Table III, where the average uniformity surpasses 77%. The main reason for uniformity decline is attributed to the limited number of unit cells in a single cycle of the metasurface, so that the coordinates of the phase transition point calculated by the proposed algorithm cannot be accurately constructed using discretized unit cells. The limitation can be addressed by incorporating a larger number of unit cells in a single cycle of the metasurface. The diffraction efficiency is determined to be more than 75%, representing the ratio of optical power projected to all desired diffraction orders to the total incident optical power. Additionally, the FOV can be adjusted by manipulating the period number of the unit cells.

Table IV provides a comprehensive comparison of the proposed method with previous related work on 2D diffraction dot array generation based on metasurfaces. In this context, *RCP* and *LCP* denote right-handed and left-handed circular polarization, respectively. Compared to prior research, the proposed method demonstrates versatility by not only achieving regular diffraction arrays with equispaced length and width but also enabling the maximization or minimization of specific orders, thereby expanding the application scope of DGs. Moreover, the proposed method achieves effective suppression of 0th order intensity, a crucial advantage for the practical application of metasurface optics. Furthermore, the simplicity of the proposed dimensions for nanorods, featuring only three different sizes, facilitates precision control in fabrication and industrial replication. This stands in contrast to numerous dimension sizes generated by conventional GS algorithms. Simultaneously, the proposed method maintains high performance with efficiency and uniformity reaching 75% and 77%, respectively. Regarding the fabrication process, the proposed DG metasurface can be fabricated through conventional electron beam lithography (EBL) coupled with etching process, thereby validating the practicality and viability of the proposed method.

IV. CONCLUSION

In conclusion, we proposed a novel polarization multiplexing DGs based on all-dielectric metasurface, demonstrating exceptional performance with efficiency and uniformity reaching 75% and 77%, respectively. The proposed method not only achieves equispaced uniform dot arrays but also broadens the application scope of DGs by accommodating specific desired target patterns. Besides, suppression of 0th order intensity is achieved, mitigating adverse effects in practical applications. The structural design of nanorods is significantly simplified, featuring only three different types of dimensions, thereby enhancing precision control in fabrication. Furthermore, the designed DG metasurface holds promise for potential integration with commercial VCSELs enabling the realization of ultra-compact miniaturized structured light system on wafer-level. Limitations of this method include the finite randomness of speckle array patterns and the continued presence of central symmetry, preventing the achievement of completely random spot array distributions. We acknowledge the potential for future research in maintaining simple metasurface parameters for ease of precision control in nanofabrication and large-scale industrial replication, while also achieving dot array patterns with arbitrary levels of randomness. We envision the proposed method offers new possibilities for practical applications including laser technology, 3D imaging, structured light projection and optical computing.

REFERENCES

- [1] H. Dammann and K. Görtler, "High-efficiency in-line multiple imaging by means of multiple phase holograms," *Opt. Commun.*, vol. 3, no. 5, pp. 312–315, 1971, doi: [10.1016/0030-4018\(71\)90095-2](https://doi.org/10.1016/0030-4018(71)90095-2).
- [2] R. L. Morrison, "Symmetries that simplify the design of spot array phase gratings," *J. Opt. Soc. Amer. A*, vol. 9, no. 9, pp. 464–471, 1992, doi: [10.1364/JOSAA.9.000464](https://doi.org/10.1364/JOSAA.9.000464).
- [3] A. Vasara et al., "Binary surface-relief gratings for array illumination in digital optics," *Appl. Opt.*, vol. 31, no. 17, pp. 3320–3336, 1992, doi: [10.1364/AO.31.003320](https://doi.org/10.1364/AO.31.003320).
- [4] C. Zhou and L. Liu, "Numerical study of dammann array illuminators," *Appl. Opt.*, vol. 34, no. 26, pp. 5961–5969, 1995, doi: [10.1364/AO.34.005961](https://doi.org/10.1364/AO.34.005961).
- [5] H. Liu et al., "Experiments and perturbative analysis of dammann-grating-based aperture filling in a passive coherent beam combination," *J. Lightw. Technol.*, vol. 32, no. 12, pp. 2220–2227, Jun. 2014, doi: [10.1109/JLT.2014.2322863](https://doi.org/10.1109/JLT.2014.2322863).
- [6] Y. Yang et al., "Dammann-grating-based passive phase locking by an all-optical feedback loop," *Opt. Lett.*, vol. 39, no. 3, pp. 708–710, 2014, doi: [10.1364/OL.39.000708](https://doi.org/10.1364/OL.39.000708).
- [7] S. Wei et al., "Binocular vision measurement using Dammann grating," *Appl. Optics*, vol. 54, no. 11, pp. 3246–3251, 2015, doi: [10.1364/AO.54.003246](https://doi.org/10.1364/AO.54.003246).
- [8] K. Liu et al., "Optimized stereo matching in binocular three-dimensional measurement system using structured light," *Appl. Optics*, vol. 53, no. 26, pp. 6083–6090, 2014, doi: [10.1364/AO.53.006083](https://doi.org/10.1364/AO.53.006083).
- [9] Y. B. Ni et al., "Metasurface for structured light projection over 120°field of view," *Nano Lett.*, vol. 20, no. 9, pp. 6719–6724, 2020, doi: [10.1021/acs.nanolett.0c02586](https://doi.org/10.1021/acs.nanolett.0c02586).
- [10] X. Huang et al., "Polarization structured light 3D depth image sensor for scenes with reflective surfaces," *Nature Commun.*, vol. 14, 2023, Art. no. 6855, doi: [10.1038/s41467-023-42678-5](https://doi.org/10.1038/s41467-023-42678-5).
- [11] A. Arbab, Y. Horie, M. Bagheri, and A. Faraon, "Dielectric metasurfaces for complete control of phase and polarization with subwavelength spatial resolution and high transmission," *Nature Nanotechnol.*, vol. 10, pp. 937–943, 2015, doi: [10.1038/nnano.2015.186](https://doi.org/10.1038/nnano.2015.186).
- [12] A. I. Kuznetsov et al., "Optically resonant dielectric nanostructures," *Science*, vol. 354, no. 6314, 2016, Art. no. aag2472, doi: [10.1126/science.aag2472](https://doi.org/10.1126/science.aag2472).

- [13] P. Qiao, W. Yang, and C. Chang-Hasnain, "Recent advances in high-contrast metastructures, metasurfaces, and photonic crystals," *Adv. Opt. Photon.*, vol. 10, no. 1, pp. 180–245, 2018, doi: [10.1364/aop.10.000180](https://doi.org/10.1364/aop.10.000180).
- [14] E. Tseng et al., "Neural nano-optics for high-quality thin lens imaging," *Nature Commun.*, vol. 12, no. 1, 2021, Art. no. 6493, doi: [10.1038/s41467-021-26443-0](https://doi.org/10.1038/s41467-021-26443-0).
- [15] X. Y. Fang, H. R. Ren, and M. Gu, "Orbital angular momentum holography for high-security encryption," *Nature Photon.*, vol. 14, pp. 102–108, 2020, doi: [10.1038/s41566-019-0560-x](https://doi.org/10.1038/s41566-019-0560-x).
- [16] Q. Dai et al., "Ultracompact, high-resolution and continuous grayscale image display based on resonant dielectric metasurfaces," *Opt. Exp.*, vol. 27, no. 20, pp. 27927–27935, 2019, doi: [10.1364/OE.27.027927](https://doi.org/10.1364/OE.27.027927).
- [17] Y. J. Bao, J. C. Ni, and C. W. Qiu, "A minimalist single-layer metasurface for arbitrary and full control of vector vortex beams," *Adv. Mater.*, vol. 32, no. 6, 2020, Art. no. 1905659, doi: [10.1002/adma.201905659](https://doi.org/10.1002/adma.201905659).
- [18] J. Deng et al., "Metasurface-assisted optical encryption carrying camouflaged information," *Adv. Opt. Mater.*, vol. 10, no. 16, 2022, Art. no. 2200949, doi: [10.1002/adom.202200949](https://doi.org/10.1002/adom.202200949).
- [19] Z. Li et al., "All-silicon nanorod-based Dammann gratings," *Opt. Lett.*, vol. 40, no. 18, pp. 4285–4288, 2015, doi: [10.1364/OL.40.004285](https://doi.org/10.1364/OL.40.004285).
- [20] S. Yang et al., "Simple and polarization-independent dammann grating based on all-dielectric nanorod array," *J. Opt.*, vol. 19, no. 9, 2017, Art. no. 095103, doi: [10.1088/2040-8986/aa7b46](https://doi.org/10.1088/2040-8986/aa7b46).
- [21] Y. Ni et al., "Metasurface for structured light projection over 120° field of view," *Nano Lett.*, vol. 20, no. 9, pp. 6719–6724, 2020, doi: [10.1021/acs.nanolett.0c02586](https://doi.org/10.1021/acs.nanolett.0c02586).
- [22] X. Zheng et al., "Visible light waveband dammann grating based on all-dielectric metasurface," *J. Appl. Opt.*, vol. 61, no. 9, pp. 2184–2191, 2022, doi: [10.1364/ao.448192](https://doi.org/10.1364/ao.448192).
- [23] Y. Wu, Z. Shi, H. Jiang, and Y. Deng, "Multi-wavelength spot-array beams based on tunable dammann grating metasurface," *Photonics*, vol. 10, no. 2, 2023, Art. no. 141, doi: [10.3390/photonics10020141](https://doi.org/10.3390/photonics10020141).
- [24] Z. L. Li et al., "Full-space cloud of random points with a scrambling meta surface," *Light: Sci. Appl.*, vol. 7, no. 1, 2018, Art. no. 63, doi: [10.1038/s41377-018-0064-3](https://doi.org/10.1038/s41377-018-0064-3).
- [25] A. Arbabi et al., "Dielectric metasurfaces for complete control of phase and polarization with subwavelength spatial resolution and high transmission," *Nature Nanotechnol.*, vol. 10, no. 11, pp. 937–943, 2015, doi: [10.1038/NNANO.2015.186](https://doi.org/10.1038/NNANO.2015.186).
- [26] N. F. Yu et al., "Light propagation with phase discontinuities: Generalized laws of reflection and refraction," *Science*, vol. 334, pp. 333–337, 2011, doi: [10.1126/science.1210713](https://doi.org/10.1126/science.1210713).